Matter

CellPress

Article

Triboiontronics for efficient energy and information flow

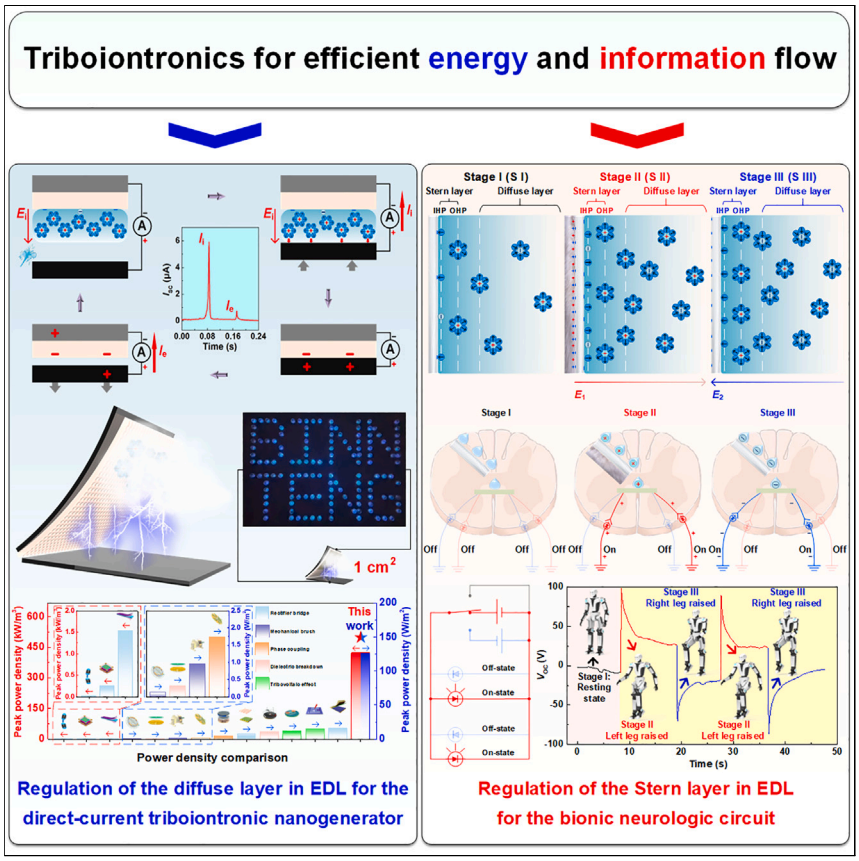

The electrical double layer (EDL) structure has been investigated for over a century, but how to fine-tune it remains a challenge. Here, dynamic regulations of EDL were achieved by contact electrification, forming triboiontronics. Through regulating the diffuse layer and Stern layer, an efficient direct-current triboiontronic nanogenerator and a bionic neurologic circuit were constructed. It provids an interdisciplinary paradigm of charge regulation for prospective applications and offers a platform to study the ionic-electronic coupling interface for efficient energy and information flow.

Xiang Li, Shaoxin Li, Xin Guo, Jiajia Shao, Zhong Lin Wang, Di Wei

zhong.wang@mse.gatech.edu (Z.L.W.)
weidi@binn.cas.cn (D.W.)

Highlights

Dynamic regulations of EDL were achieved by CE to form triboiontronics

DC-TING with 126.40 W/m^2 was constructed via adjustment of the diffusion layer

The bionic neurologic circuit was built up via adjustment of the Stern layer

The polarity, quantity, and type of charge were fine-tuned in triboiontronics

1 **Discovery**
A new material or phenomena

Li et al., Matter 6, 3912–3926
November 1, 2023 © 2023 Elsevier Inc.
https://doi.org/10.1016/j.matt.2023.08.022

CellPress

Matter

Article

Triboiontronics for efficient energy and information flow

Xiang Li,[1,2] Shaoxin Li,[1] Xin Guo,[1,2] Jiajia Shao,[1] Zhong Lin Wang,[1,3,*] and Di Wei[1,4,*]

SUMMARY

Information flow in the central nervous system consumes little energy, and nerve impulses are carried through by the conduction of ions within the electrical double layer (EDL). The EDL structure has been investigated for over a century, but how to fine-tune it remains a challenge. Here, dynamic regulations of the EDL at the dielectric-liquid interface were achieved by contact electrification (CE), forming triboiontronics. Firstly, the ionic charge density in the nano-confined diffuse layer was regulated by CE-induced charge, enabling a direct-current triboiontronic nanogenerator (DC-TING) with an ultra-high peak power density of 126.40 W/m^2. Furthermore, the charge distribution in the sub-nanoconfined Stern layer was adjusted by CE-induced electric fields, achieving bidirectional ionic-electronic signal conversion for a bionic neurologic circuit. Through dynamic EDL regulation in triboiontronics, the polarity, quantity, and type of charge were fine-tuned, which provided a versatile paradigm for various prospective applications in efficient energy harvesting and neuromorphic computing.

INTRODUCTION

From the ubiquitous Internet of Things (IoT) to highly integrated human brains, energy efficiency plays a critical role in the flow of information.[1,2] The IoT consists of numerous electronic sensors, and the conventional von Neumann computing architecture in electronics is facing challenges with the end of Moore's law, which have become even more severe in today's era of big data.[3] To satisfy our ever-growing appetite for data and information, a more efficient neuromorphic computing paradigm is desperately needed. Brain activation could be defined as the information-driven reorganization of energy flows in a population of neuroglial units that leads to an overall increase in energy utilization.[4,5] Inspired by the human brain, new concepts of iontronics have aroused great research interests in exploring diverse neuromorphic devices.[6–8] Unlike electronics that use only electrons and/or holes as the primary charge carriers, iontronics couples ionic/electric charge transfer and exchange signals at the coupling interface, which has much higher energy efficiency.[9] For example, the human brain as a typical highly integrated iontronic center processing unit consumes only 12 W; however, it takes tens of megawatts to build a brain-like integrated electronic system.[10] In iontronics, the electrical double layer (EDL) controls electronic properties through ion transport and rearrangement, and it could provide an alternative paradigm to provide efficient energy and information flow required by the post-Moore era.[11]

Although the EDL has been directly used in high-power supercapacitors,[12,13] it has more essential roles in both information flow in the central nervous system and the formation of the solid electrolyte interface (SEI) in batteries.[14,15] Recent studies

PROGRESS AND POTENTIAL

In the Internet of Things, energy efficiency plays a critical role in the flow of information. The Neumann computing architecture in traditional electronics faced challenges with the end of Moore's law. Inspired by the human brain, diverse neuromorphic iontronics offers an alternative paradigm to provide efficient energy and information flow by ionic charge carriers, in which the electrical double layer (EDL) is essential. Here, the dynamic regulation of charge carriers in EDL was achieved by contact electrification, forming triboiontronics. Through regulating the nanoconfined diffuse layer and sub-nanoconfined Stern layer, an efficient direct-current triboiontronic nanogenerator and bionic neurologic circuit were constructed. It provides an interdisciplinary paradigm of charge regulation for various prospective applications and offers a platform to study the ionic-electronic coupling interface for efficient energy and information flow.

showed clearly that the dynamic ionic-electronic coupling interaction of EDL at the nanoscopic level determines the physiochemical properties of the SEI, influencing the performance of most batteries.[15] Therefore, charge carriers' interaction of EDL at the nanoscopic level determines the performance of macroscopic devices. Thus, understanding the EDL formed at the solid-liquid/liquid-liquid interface is critical in many fields, from neuroscience, energy storage, and catalysis to colloid formation.[16–18] The study of the structure and composition of the EDL has continued for over a century since the first Helmholtz's flat model was proposed.[19–23] Most EDL structure models were proposed based on a conductor-liquid system, in which the dynamic EDL could be adjusted by electrochemistry. In this case, various electrochemical techniques could fine-tune the rate of chemical reactions by an electroinductive effect in the EDL.[24,25] However, if the solid is an insulator, there seems little means to control the dynamic adjustment in the EDL at the dielectric-liquid interface. A "two-step" model was recently proposed for the formation of the EDL for an insulator liquid,[26–28] in which the electrons firstly transfer between the dielectric insulator and the water when the liquid contacts the solid surface, and the ionization reaction that occurs on the solid surface attracts the opposite ions in the liquid by electrostatic interaction.

In this article, dynamic regulations of charge carriers in the diffuse layer and the Stern layer in the EDL at the dielectric-liquid interface were realized, respectively, by means of contact electrification (CE), forming triboiontronics. It could adjust the ionic-electronic coupling interface to achieve highly efficient energy harvesting and information transmission. Firstly, the ionic charge density in the nanoconfined diffuse layer on the dielectric insulator could be adjusted by pre-charged deionized (DI) water mist induced by solid-liquid CE, which creates a built-in electric field in the direct-current triboiontronic nanogenerator (DC-TING) to couple the ionic current with the electric displacement current, developing DC output. Compared with the conventional triboelectric nanogenerator (TENG), the DC-TING as a triboiontronic device based on the *in situ* ionic charge supplement strategy could maintain a high charge density on the dielectric insulator. It achieved an ultra-high peak power density of 126.40 W/m^2 (421.33 kW/m^3) at 0.10 Hz, where the output performance of most TENGs is weak. Furthermore, the ionic charge polarity of the diffuse layer could also be remotely adjusted through dynamic regulation of the charge distribution in the sub-nanoconfined Stern layer by bidirectional electric fields generated by solid-solid CE. The bionic neurologic circuit was realized, and it transfers triboiontronic information from CE with ionic charge polarity information stored in the diffuse layer to be converted into the corresponding electronic signal. It could be used to build a source-free human-computer interaction interface for neuromorphic self-powered in-sensor computing systems. Therefore, the realization of the triboiontronics by a source-free dynamic regulation EDL not only can provide a new paradigm for highly efficient energy harvesting and information transmission but also can provide a paradigm of multi-faceted regulation of the polarity (positive or negative), quantity, and type (ionic or electric) of charge for wide prospective applications.

RESULTS AND DISCUSSION

High-power DC-TING via regulation of the diffuse layer in EDL

When DI water is in contact with the insulator, the formed EDL includes a negatively charged Stern layer with a sub-nanometer-level thickness and a positively charged diffuse layer with a nanometer-level thickness. The ionic charge density of the diffuse layer could be dynamically adjusted by the pre-charged DI water mist induced by the solid-liquid CE. It could construct a built-in electric field in the TENG to generate

[1]Beijing Institute of Nanoenergy and Nanosystems, Chinese Academy of Sciences, Beijing 101400, China

[2]School of Nanoscience and Engineering, University of Chinese Academy of Sciences, Beijing 100049, China

[3]Georgia Institute of Technology, Atlanta, GA 30332-0245, USA

[4]Lead contact

*Correspondence: zhong.wang@mse.gatech.edu (Z.L.W.), weidi@binn.cas.cn (D.W.)

https://doi.org/10.1016/j.matt.2023.08.022

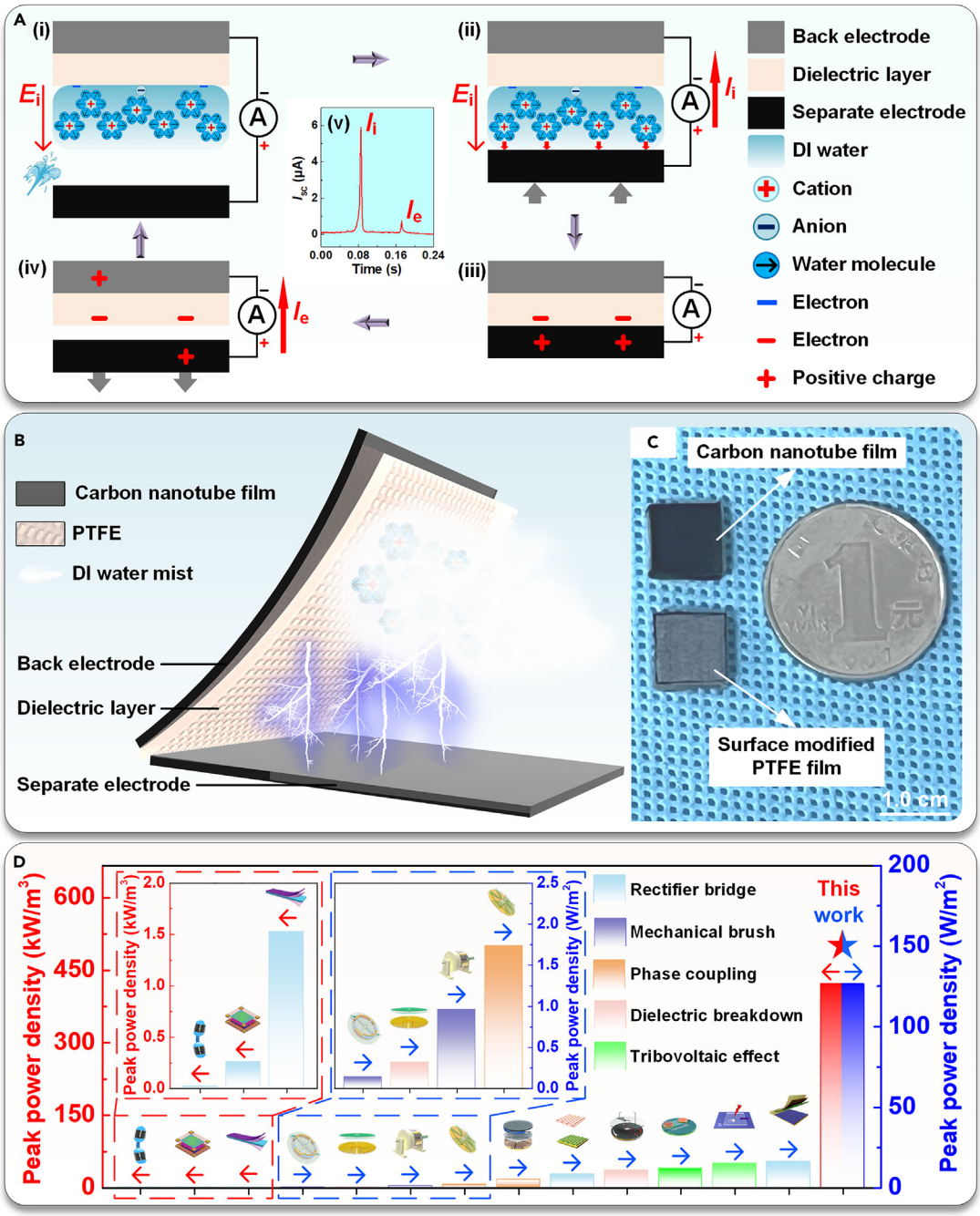

Figure 1. DC-TING based on the dynamic regulation ionic charge density of the diffuse layer in EDL by CE

(A) The regulation principle of the diffuse layer and the operation principle of DC-TING.

(B) Schematic diagram of DC-TING.

(C) Physical appearance of DC-TING.

(D) The peak power density comparison of DC-TING with other representative works.

ionic current coupling the electronic displacement current, developing the triboiontronic DC-TING. Its regulation mechanism is shown in Figure 1A. Firstly, the DC-TING was in a separation state, as shown in Figure 1Ai, and the pre-positive charged DI water was sprayed on the dielectric layer to form the EDL. The cations in the mist

efficiently increased the positive charge density in the nanoconfined diffuse layer, thereby constructing a built-in electric field, E_i. The positive charges in the DI water were generated from the solid-liquid CE within the humidifier (Figure S1A). Compared with the constant I_{SC} of about 0.4 μA generated from the DI water mist, the I_{SC} generated from 1 M LiCl aqueous solution mist was 0 μA (Figures S1B and S1C). This proved that the higher concentration of free ions in the solution might have caused the screen effect[28] that prevented the water mist from being pre-charged and that the charge in the mist originated from the solid-liquid CE instead of from the current leakage from the humidifier. Secondly, when the separate electrode gradually approached the dielectric layer with the positively charged water film, the electrostatic induction would be caused by the positive charge. The direction of the electronic displacement current generated by the positively charged polytetrafluoroethylene (PTFE) surface was opposite to that caused by the negatively charged PTFE surface (Figure S2). So, during the contact process, the electrons were gradually transferred from the back electrode to the separate electrode, forming a small electronic contact displacement current. Once the diffuse layer was in contact with the separate electrode, positive charges in the diffuse layer would be rapidly transferred onto the separate electrode surface under the action of E_i, generating a larger ionic current, I_i, as shown in Figure 1Aii. The electronic contact displacement current during the contact process was in the same direction as the I_i. Thirdly, the macroscopic water film was observed to be completely squeezed out of the DC-TING. When the dielectric layer contacted the separate electrode, electrons from the separate electrode were transferred to the dielectric layer surface (Figure 1Aiii). Fourthly, the dielectric layer was separated from the separate electrode, based on the principle of electrostatic induction, and electrons from the back electrode were transferred to the separate electrode to generate the electronic displacement current I_e (Figure 1Aiv). As shown in the comparison diagram of the waveforms of I_i and I_e (Figure 1Av), both were in the same direction, and DC ionic-electronic coupling output was generated by the DC-TING. Finally, when the DC-TING was in a separation state again, the pre-positively charged DI water was re-sprayed on the dielectric layer to form the fresh EDL. The DC-TING entered the stage of Figure 1Ai again, thus achieving continuous and stable output. As the ionic charge density of the diffuse layer on the dielectric layer can be enhanced by increasing surface area, DC-TING was designed to comprise both the separate electrode and the back electrode made of carbon nanotube film (Figure 1B). It not only had a larger surface area for collecting more ionic charges but also could prevent being oxidized in humid environments to maintain the operational stability of the DC-TING. The dielectric layer covered on the back electrode was made of PTFE film. The physical appearance of the DC-TING is shown in Figure 1C.

The DC-TING could achieve DC output to directly supply power to electronics without the assistance of the rectifier bridge. In contrast to the TENG based on the coupling effect of CE and electrostatic induction (Figure S3), the DC-TING can not only reduce the additional energy consumption by the rectifier bridge but can also have prospects in more power-hungry applications. Compared with other types of DC-TENGs including mechanical brush,[29,30] phase coupling,[31,32] dielectric breakdown,[33,34] and tribovoltaic effect,[35,36] the DC-TING effectively solved major drawbacks such as low robustness of complex construction, wasted energy due to multiple rectifier bridges, high requirement on charge density, rapid loss of space charge region as in semiconductors, etc. More importantly, based on the *in situ* ionic charge supplement strategy from the pre-charged DI water mist, the DC-TING could achieve self-charge-replenishment capability, thereby maintaining a high charge density on the PTFE dielectric layer surface, resulting in ultra-high-power density.

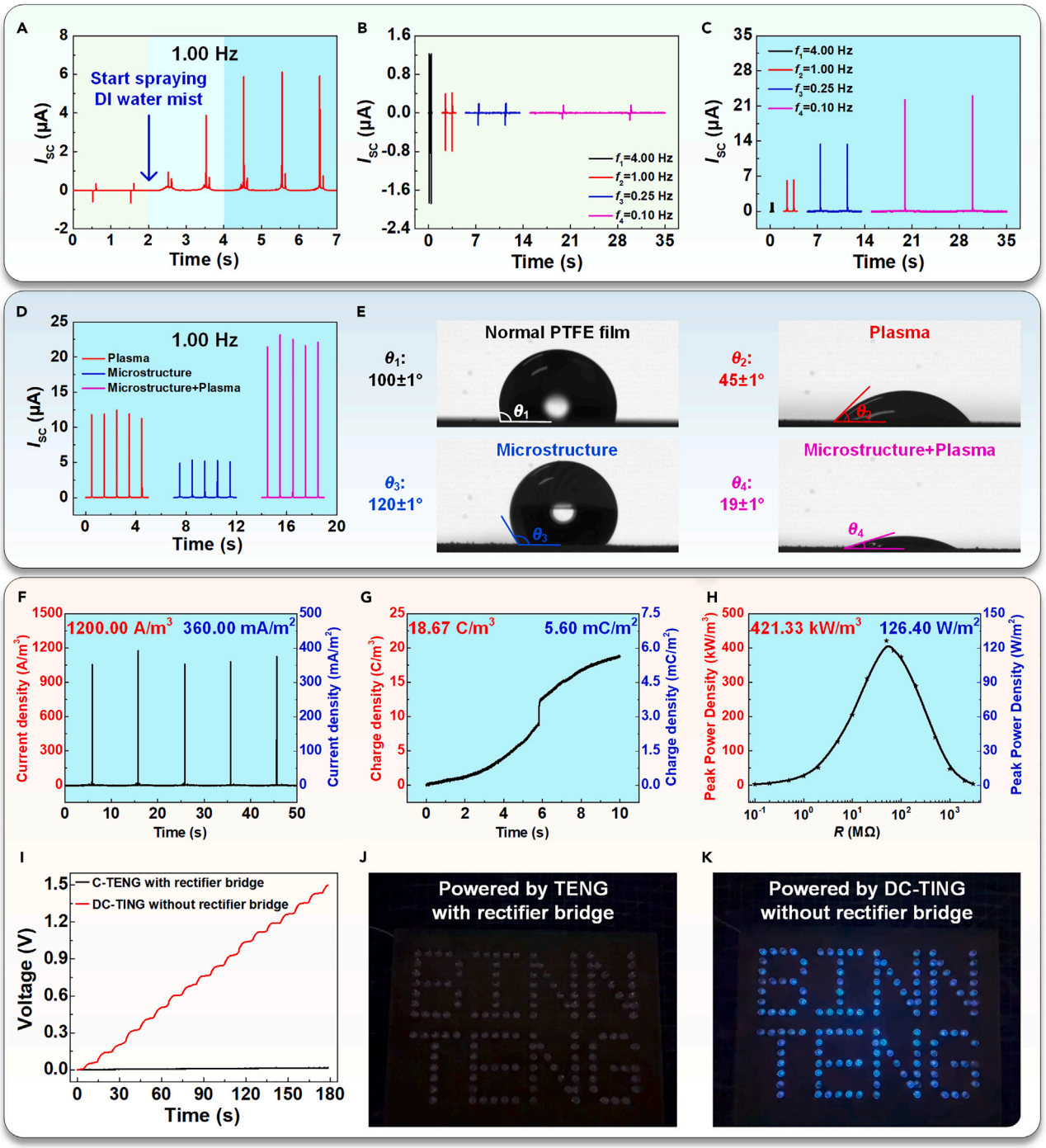

Figure 2. The output performance and application display of DC-TING

(A) When the positively ionic-charged DI water was sprayed on the PTFE film, the changing process of I_{SC} of DC-TING.

(B) I_{SC} of TENG at different frequencies.

(C) I_{SC} of DC-TING at different frequencies.

(D) I_{SC} of DC-TING with different surface treatments on PTFE film.

(E) Hydrophilicity test of PTFE film with different surface treatments.

(F) The short-circuit current density of DC-TING.

(G) The transferred charge density of DC-TING.

(H) The peak power density of DC-TING.

Figure 2. *Continued*
(I) Comparison of charging rates for the capacitor.
(J) The LED board was powered by TENG with the assistance of a rectifier bridge.
(K) The LED board was powered by DC-TING.

It does not require extreme environmental conditions and stringent requirements on materials, in contrast to other ways to increase the charge density at the interface including pumping up the charge density by charge shuttling,[37] via repeated rheological forging,[38] or suppressing surface charge decay in a high vacuum[39] or in a high-pressure gas environment.[40] As a comparison, the peak power densities of representative works based on various existing rectification methods are shown in Figures 1D and S4. Among them, the ultra-high peak power density of the DC-TING is 126.40 W/m^2 (421.33 kW/m^3), which is several orders of magnitude over its TENG peers, thereby making a great breakthrough.

To verify the operation principle of DC-TING, the experiment was carried out in Figure 2A. In the dry state (no water mist was sprayed on the PTFE film), the DC-TING was converted to a TENG, which generated an electronic short-circuit current (I_{SC}) in alternating current (AC) form of 0.8 μA at 1 Hz. In the operating state (the pre-charged DI water was sprayed onto the PTFE film), the DC-TING started to output I_{SC} in DC form. As the ionic charge accumulated, I_{SC} continued to increase to about 6 μA. In addition, the methods of non-contact operation (Figure S2) and oil-dripping experiment (Figure S5) were used to keep the ionic charge always on the PTFE film surface without transferring it to the separate electrode. In the above cases without I_is, the positively charged mist film was always covered on the PTFE dielectric layer either by the distance in the non-contact operation or by the oil layer, so the surface electric property was kept positive. Thus, the DC-TING was converted to a TENG to generate AC signals, and the signal direction was opposite to that of the TENG in the dry state, in which the surface electric property on the PTFE dielectric layer was negative. The results obtained from the above experiments proved that DC-TING can produce DC ionic-electronic coupling output by adjusting the charge density of the diffuse layer in the EDL. When different types of electrolyte solutions were sprayed on the surface of the dielectric layer, the DC-TING generated weaker AC electric signals (Figure S6). It showed that a higher concentration of free ions could quickly form a compact EDL and that the screening effect of it would weaken the dynamic regulation of ionic charge density of the diffuse layer in the EDL by CE.

Different replenishment strategies of ionic charge were further studied in detail. Firstly, the influence of charge replenishment time on DC-TING output was studied. In the dry state, the electronic outputs of the TENG were reduced with decreasing operating frequency (Figures 2B, S7A, and S7B). As the operating frequency decreased from 4 to 0.10 Hz, the I_{SC}, transferred charge (Q_{SC}), and open-circuit voltage (V_{OC}) correspondingly reduced from 1.9 μA, 5.2 nC, and 13 V to 0.2 μA, 3.3 nC, and 8 V, respectively, whereas DC-TING outputs were effectively increased with decreasing frequency (Figures 2C, S7C, and S7D). As the operating frequency changed from 4 to 0.10 Hz, I_{SC}, Q_{SC}, and V_{OC} increased from 1.8 μA, 19.7 nC, and 115 V to 22.2 μA, 450.0 nC, and 1,300 V, respectively. The strategy of extending charge replenishment time by reducing the operating frequency could allow more pre-charged DI water to be sprayed on the dielectric layer, thereby effectively increasing the ionic charge accumulation in the diffuse layer to improve the DC-TING output. The V_{OC} of the DC-TING was too high to be tested directly, but it could be calculated by Ohm's law approximately through testing the internal resistance (Figure S7E), by connecting the external load in series in the equivalent circuit to

test the load current (I_R in Figure S7F). Compared with the TENG, based on such an *in situ* ionic charge supplement strategy, the DC-TING could avoid the depletion of induced charges on the dielectric layer surface in a high-humidity environment,[41] ensuring stable output performance in different humidity environments (Figures S8). Secondly, the effect of increasing the hydrophilic area of the dielectric layer on DC-TING output was studied. The outputs were compared after the PTFE film was modified by three methods of plasma sputtering, microscopic engraving (Figure S9A), and a combination treatment of microscopic engraving followed by plasma sputtering. After comparison, the DC-TING with the PTFE film modified by combination treatment had the best output performance (I_{SC}, Q_{SC}, I_R, and V_{OC}) at 1 Hz with 23.5 μA, 410 nC, 1.25 μA, and 1,250 V (Figures 2D and S9B–S9D), compared with plasma sputtering (12.5 μA, 145 nC, 0.72 μA, and 720 V) and microscopic engraving (5 μA, 48 nC, 0.30 μA, and 300 V). The hydrophilicity test showed that the DI water droplets on the PTFE film with the combination treatment had the smallest contact angle of 19° (Figure 2E), in contrast to that of the normal PTFE film (100°) and the other two treatment methods (45° and 120°). Therefore, the strategy of increasing the hydrophilic surface area on the dielectric layer surface could increase the ionic charge storage capacity, resulting in the improvement of DC-TING output.

Combining the above ionic charge replenishment strategies, the DC-TING can maintain a high charge density on the dielectric layer for efficient output. Its I_{SC}, Q_{SC}, V_{OC}, and peak power (P_R) could achieve 36 μA, 560 nC, 1,750 V, and 12.64 mW at 0.10 Hz (Figures S10A–S10D). By calculation, the DC-TING had an ultrahigh I_{SC} density of 1,200 A/m^3 and 360 mA/m^2, a transferred charge density of 18.67 C/m^3 and 5.60 mC/m^2, and a peak power density of 421.33 kW/m^3 and 126.40 W/m^2 (Figures 2F–2H). To verify the practicality of such a high-power DC-TING, firstly, the charging capacities of different generators for a 22 μF capacitor were compared at 0.10 Hz (Figure 2I). It is almost impossible for the TENG to charge the capacitor only by relying on electronic output even with the assistance of the rectifier bridge, but the DC-TING could directly charge it to 1.5 V in only 18 operating cycles without the rectifier bridge. Secondly, the internal capacitances of different generators were tested (Video S1). The equivalent circuit of TENG consisted of the series-connected voltage source and an adjustable ordinary capacitor,[42,43] and its internal capacitance value was 6.7 pF (Figure S11A), while in the DC-TING, the pre-charged DI water on the dielectric layer converted the ordinary capacitor into the supercapacitor-like model to increase the capacitance value, which reached 31.6 pF (Figure S11B). So, the DC-TING could directly increase the internal capacitance value without a complex circuit design to improve the output. Thirdly, the comparison of different generators powering the light-emitting diode (LED) board is shown in Video S2. By relying on purely electronic output, the TENG could not drive the LED board with the assistance of the rectifier bridge (Figures 2J and S11C), but the DC-TING could directly drive the LED board to work normally (Figures 2K and S11D). Therefore, compared with the TENG, the DC-TING could not only eliminate the limitation of the rigid rectifier bridge but could also achieve excellent performance in practical applications with highly efficient energy-harvesting capability.

Bionic neurologic circuit via regulation of the Stern layer in EDL

Besides regulating the ion charge density of the diffuse layer in the EDL to create the DC-TING, its ionic charge polarity could also be effectively remotely adjusted through dynamic regulation of the charge distribution in the sub-nanoconfined Stern layer by bidirectional electric fields generated by solid-solid CE. In stage I, the DI

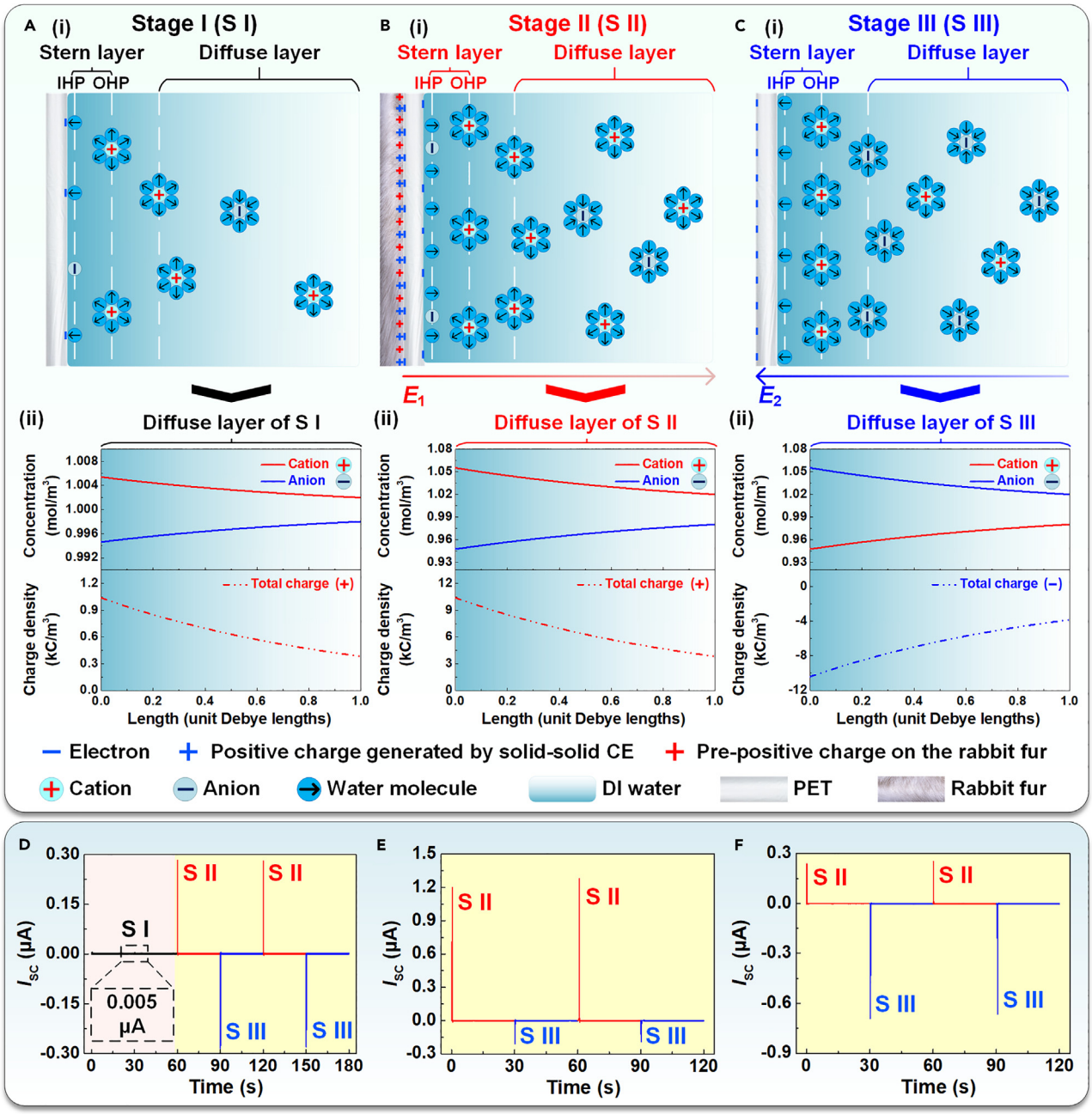

Figure 3. Dynamic regulation of the charge distribution of the Stern layer in EDL

(A) The EDL in stage I when DI water was in contact with the PET film.

(B) The EDL in stage II when the rabbit fur with positive charges was brought in contact with the PET film.

(C) The EDL in stage III when the rabbit fur was removed.

(D) I_{SC} generated by DI water mist in different stages.

(E) Increased I_{SC} generated by DI water mist in stage II through increasing pre-positive charges of rabbit fur.

(F) Increased I_{SC} generated by DI water mist in stage III through increasing electrons transferred from rabbit fur to PET film.

water was in contact with the polyethylene terephthalate (PET) film (Figure 3Ai). Based on the "two-step" model of the EDL,[26–28] electrons transferred from water to the PET film surface, and the ionization reaction occurred at the same time. Both the electrons and anions were adsorbed on the PET surface to form a negatively

charged inner Helmholtz plane (IHP), and water molecules were polarized to form a dipole layer on the PET film surface. Then, a small number of hydrated cations in water would be attracted by IHP to form the outer Helmholtz plane (OHP) by electrostatic interaction. IHP and OHP together formed the Stern layer with a negative total charge. According to the Gouy-Chapman-Stern theory,[20–22] the diffuse layer in the EDL is considered a multi-physics coupling of the Nernst-Planck and Poisson equations (Poisson-Nernst-Planck equation), where the Nernst-Planck equation describes the mass transfer of ions and the Poisson equation describes the charge density and electric field. To determine the charge polarity of the diffuse layer, concentrations c_i (SI unit: mol/m^3, $i = +,-$) of opposite ionic charges need to be simulated, and its relationship with the fluxes $\mathbf{J}_i$ (SI unit: mol/(m^2·s)) can be expressed as

$$\mathbf{J}_i = -D_i\nabla c_i - u_{m,i}z_iFc_i\nabla\varphi, \quad \text{(Equation 1)}$$

where D_i (SI unit: m^2/s) is the diffusion coefficient, $u_{m,i}$ (SI unit: s·mol/kg) is the mobility, z_i is the charge of ions, F (SI unit: C/mol) is the Faraday constant, and φ (SI unit: V) is the electric potential in the diffuse layer. Assume that there are no homogeneous reactions of the ions in the solution. Then, conservation of mass requires that for both species

$$\nabla\cdot\mathbf{J}_i = 0. \quad \text{(Equation 2)}$$

For the potential, the Poisson equation shows that

$$\nabla\cdot(-\varepsilon\nabla\varphi) = \rho, \quad \text{(Equation 3)}$$

where ε is the permittivity (SI unit: F/m) and ρ is the total charge density (SI unit: C/m^3), which depends on the ion concentration

$$\rho = F(c_+ - c_-) \quad \text{(Equation 4)}$$

Based on the correlation of the above equations, the cation concentration (c_+), the anion concentration (c_-), and the total charge density (ρ) of the diffuse layer could be simulated by COMSOL Multiphysics 6.1, and the specific simulation model and parameters are shown in Figure S12 and Table S1. The simulation results showed that in the EDL, the ionic charge polarity of the diffuse layer was opposite to the charge polarity of the Stern layer, and the total charge density decreased with increasing distance from the solid surface. As in stage I (Figure 3Aii), the cation concentration was slightly higher than that of the anion in the diffuse layer, resulting in a weak positive total charge density. In stage II, the rabbit fur with pre-positive charges was brought in contact with the PET film to generate the solid-solid CE effect. Based on the electronegativity difference, electrons were transferred from the fur to the film surface (Figure 3Bi). The pre-charged fur generated a positive electric field of E_1. Based on the electrostatic induction, the E_1 could promote more electrons transferred from water to the PET film surface, and it attracted more anions with the lower hydration-free energy escaping from the hydration shell to adsorb on the film surface. So, a more compact IHP was formed. Then, hydrated cations in water would be attracted to form OHP. Thereby, the Stern layer with a stronger negative total charge was formed. According to the simulation results, the cation concentration was much higher than that of the anion in the diffuse layer, resulting in a higher positive total charge density (Figure 3Bii) opposite to the total charge of the Stern layer. In stage III, the rabbit fur was removed (Figure 3Ci). The transferred electrons by solid-solid CE were retained on the PET film surface to generate a negative electric field E_2, which would attract cations in the DI water to the vicinity of the film surface. However, due to the high hydration-free energy, cations usually could not escape from the hydration shell to enter the water molecular dipole layer, and they could not directly adsorb on the PET film surface.[44] So, the IHP was mainly constituted

by the water molecular dipole layer, and the hydrated cations formed the OHP, forming the Stern layer with a stronger positive charge. Simulation results also showed that the concentration of anions was much higher than that of the cations in the diffuse layer, resulting in higher negative total charge density (Figure 3Cii) opposite to the total charge of the Stern layer. Therefore, by simply adjusting the solid-solid CE between the PET film and the rabbit fur, the charge distribution of the Stern layer and the ionic charge polarity (positive or negative) of the diffuse layer in the EDL could be remotely regulated without an external power source.

To verify the above mechanism, experimental verification was further carried out, and a PET sprayer with a single spray volume of approximately 1 mL was selected. In Figure 3D, without solid-solid CE, the I_{SC} generated from pure DI water mist was only 0.005 μA, representing stage I. However, when solid-solid CE was applied, i.e., the rabbit fur was in contact with the PET sprayer, an I_{SC} of 0.28 μA was generated in stage II. Once the fur was removed, it changed to −0.28 μA as defined in stage III. The Q_{SC} (1.2, 40, and −40 nC) and V_{OC} (2, 59, and −59 V) followed a similar trend in the corresponding stages (Figures S13A and S13B). Differences in electric signals in different stages proved that the ionic charge polarity of the diffuse layer was effectively adjusted by CE, even if it could be realized with the remote control method by CE (Figure S14). Compared with the Q_{SC}s of 40 and −40 nC generated by the sprayed DI water mist in stages II and III, the Q_{SC}s from the sprayed 1 M LiCl aqueous solution mist in the corresponding stage were reduced to 0.9 and −0.9 nC, respectively (Figure S15). It proved that the compact EDL generated by a higher concentration of free ions in the electrolyte solution could weaken the dynamic regulation of the charge distribution in the Stern layer by CE. A further experiment was carried out by using rabbit fur pre-rubbed against the PTFE film to induce more positive charges on the fur. Then, when the pre-rubbed fur contacted with the PET sprayer (Figure S16A), positive electric signals of the water mist were increased in stage II (I_{SC}, Q_{SC}, and V_{OC} were increased to 1.20 μA, 180 nC, and 280 V, respectively) (Figures 3E and S16C). It demonstrated the positive ionic charge of the diffuse layer in stage II was induced by the positive electric field caused by pre-positive charges on the rabbit fur. On the other hand, using the pristine rabbit fur to rub against the PET sprayer 10 times allowed more electrons to be transferred to the PET surface (Figure S17A). It could correlatively increase the negative electric signals of the water mist in stage III (I_{SC}, Q_{SC}, and V_{OC} were increased to −0.70 μA, −100 nC, and −150 V, respectively) (Figures 3F, S17B, and S17C). So, the negative ionic charge of the diffuse layer in stage III was induced by the negative electric field caused by electrons transferred from the rabbit fur to the PET film. According to the comparison of electric signals generated by the sprayed DI water mist at different stages, it could be seen that the regulations in different stages did not interfere with one other.

Nerve fibers inside the central nervous system were related to the EDL when transmitting action potentials[45] and the opening of ionic channels between cells was regulated by the EDL on the surface of the cell membrane.[46] Referring to the control mode of the human central nervous system, the dynamic regulation of the ionic charge polarity in the diffuse layer by CE could be used to construct a triboiontronic circuit to achieve a similar control mode. The neurologic circuit in which the brain controls the body's movement of walking is shown in Figures 4Ai and 4Aii. It achieved accurate transmission of information from the central nervous system and controlled coordinated motion of lower limbs with lower energy consumption. If similar control functions were realized by electronic circuits, it was necessary to build a complex circuit containing multiple diodes with external power sources

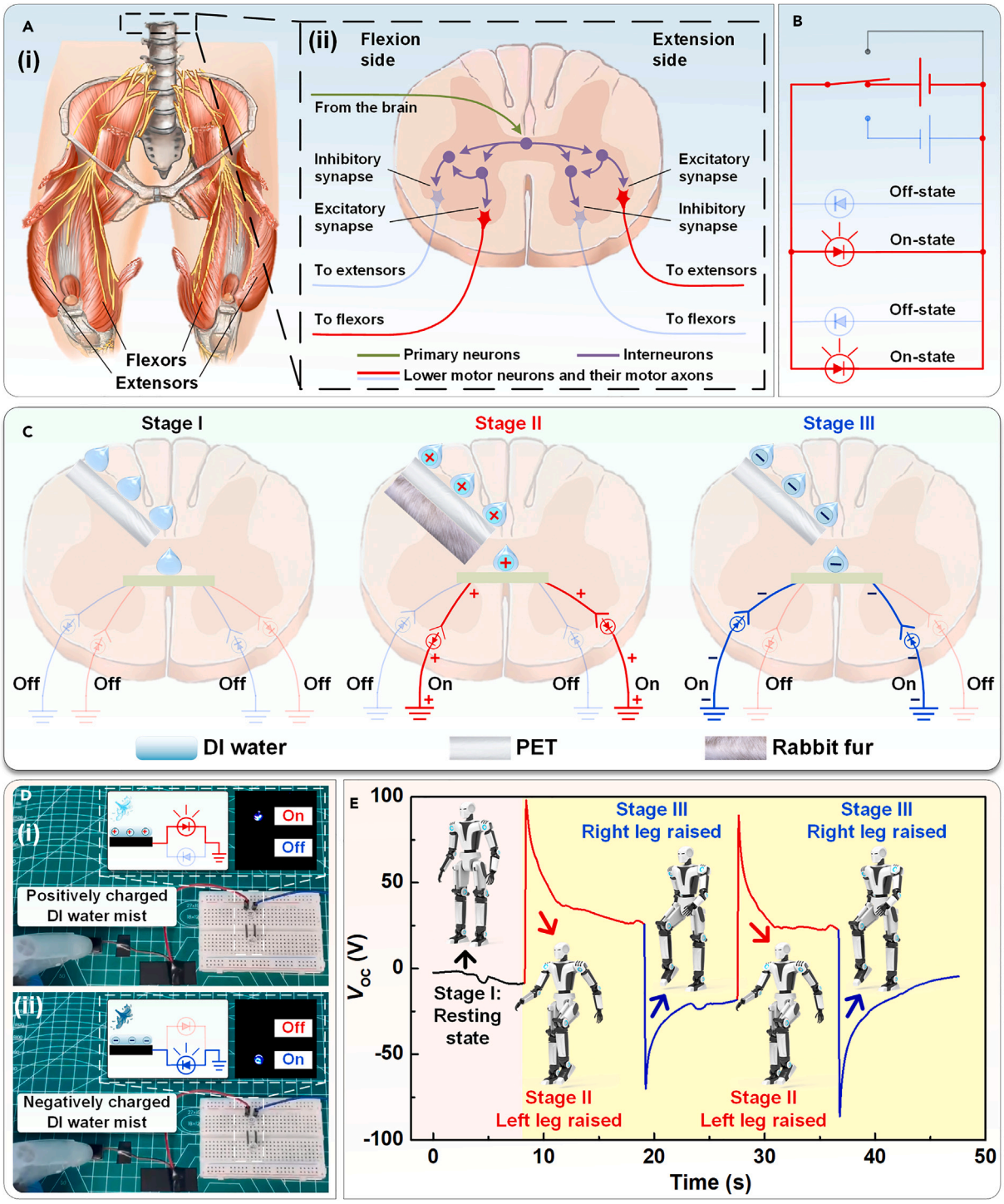

Figure 4. Triboiontronic bionic neurologic circuit and its applications

(A) Coordinated control of limb movements by the human brainstem: (i) flexors and extensors of human lower limbs and (ii) human central neurologic circuit.

(B) The electronic circuit that can achieve coordinated control.

(C) Bionic neurologic circuit based on the regulation of the ionic charge polarity of the diffusion layer.

(D) Demonstration of the regulation of the ionic charge property of DI water in the diffuse layer: (i) positive ionic charges in the diffuse layer in stage II induced positive electron currents, and (ii) negative ionic charges in the diffuse layer in stage III induced reverse electron currents.

(E) Demonstration of the bionic neurologic circuit for achieving rhythmic coordinated control of robots.

(Figure 4B). However, it is much simpler and more efficient in the triboiontronic bionic neurologic circuit (Figure 4C). Firstly, when the rabbit fur with positive charges was not in contact with the initial PET film in stage I, the DI water was dropped on the electrode, external circuits were all in the disconnected state, and the bionic circuit was analog to the resting state. Next, when rabbit fur with positive charges was in contact with the PET film in stage II, the dropped DI water with a larger positive ionic charge could induce the forward electronic current in external circuits that were highlighted with red color. Finally, when the rabbit fur was removed in stage III, the dropped DI water with a larger negative ionic charge could induce the reverse electronic current in external circuits that were highlighted with blue color. Therefore, in the bionic neurologic circuit, the ionic charge polarity of the diffuse layer could be adjusted by simple CE to transfer perceived physical contact information and induce the coordinated generation of bidirectional electronic currents, without external power. Through the EDL, it could not only transmit information but could also realize the perfect rhythmic alternating control for induced bidirectional electronic currents, analogous to the neurologic circuit.

To demonstrate the dynamic regulation capability for the charge distribution in the Stern layer, the bionic neural circuit was used to control different LEDs to work alternately without external power (Video S3). In stage II, when the PET sprayer was wrapped in positively charged rabbit fur, the DI water mist sprayed by it could only light the forward LED (Figure 4Di). While the fur was removed in stage III, the DI water that was sprayed again could directly light the reverse LED (Figure 4Dii). Based on this adjustment principle, analogous to the simple control of the human neurologic circuit, the bionic neurologic circuit had a wide range of application scenarios. As an intuitive display, it controlled the red and blue LEDs to operate alternately, as shown in Figure S18. In addition, using the bionic neurologic circuit, it could control the virtual robot to perform the walking motion, as shown in Figure 4E and Video S4. In stage I, the bionic circuit in the resting state keeps the virtual robot stationary. Then, by simply adjusting the contact states between the rabbit fur and PET sprayer in stages II–III, the sprayed DI water with different ionic charge polarity could directly control the virtual robot to carry out the multi-degree-of-freedom rhythmic coordinated motion. The bionic neurologic circuit first transferred perceived physical contact information across the medium, converted it into different ionic charge polarities in the diffuse layer, and, finally, converted it into the corresponding electronic signals. Compared to highly sophisticated silicon-based chips, the ionic-electronic coupling in triboiontronics offers a simple, safe, and effective human-computer interaction interface without an external power source. By integration of triboiontronic logic circuits with distributed parallel processing capability and good biocompatibility, self-powered in-sensor computing systems, implantable neuronal-computer interfaces, and diverse low-power neuromorphic devices could be enabled with numerous more advanced functions.

Conclusions

In summary, triboiontronics that could dynamically regulate charge carriers in the EDL at the dielectric-liquid interface was realized by means of CE in this article, achieving highly efficient energy harvesting and self-powered information transmission. Firstly, the ionic charge density of the diffuse layer in the EDL on the dielectric layer could be adjusted by positively pre-charged DI water mist induced by solid-liquid CE, which created an E_i in the DC-TING to generate an efficient DC ionic-electronic coupling output, providing one of the first trials to use I_i to rectify I_e in a TENG. It also opened a new scenario to investigate the influence of the EDL in the TENG, offered unique benefits to avoid the depletion of induced charges, and improved

its peak power density significantly, resulting in an ultra-high peak power density of 126.40 W/m^2 (421.33 kW/m^3) at 0.10 Hz that was several orders of magnitude over equivalent TENGs. Furthermore, the dynamic conversion of charge distribution in the Stern layer was realized by bidirectional electric fields generated from solid-solid CE, which can remotely control the ionic charge polarity of the diffuse layer. A bionic neurologic circuit was built in which the triboiontronics transferred perceived physical contact information from CE to ionic charge polarity information stored in the diffuse layer to generate bidirectional electronic signals without external power. This demonstrated the possibility to build a source-free human-computer interaction interface by both experiments and theoretical modeling from COMSOL Multiphysics. Through dynamic regulation of the EDL, the type (ionic or electric), polarity, and quantity of charge could be tuned. This provides an interdisciplinary paradigm of charge regulation for various prospective applications and offers a platform to study the ionic-electronic coupling interface in triboiontronics for efficient energy and information flow.

EXPERIMENTAL PROCEDURES

Resource availability

Lead contact

Further information and requests for resources and reagents should be directed to and will be fulfilled by the lead contact, Di Wei (weidi@binn.cas.cn).

Materials availability

The materials generated in this study are available from the lead contact upon reasonable request.

Data and code availability

The data used to support the findings of this study are available from the lead contact upon reasonable request.

Materials

Carbon nanotube films were synthesized by floating catalyst chemical vapor deposition growth method. A solution of ethyl alcohol of absolute ethyl alcohol with 1.2 vol % ferrocene and 0.4 vol % thiophenes carried by Ar/H_2 was injected at a rate of 20 mL/h into a horizontal furnace and atomized at 1,300°C. Under this condition, carbon nanotubes spontaneously form a continuous sock-like aerogel in the airflow, which can be blown out by the carrier gas. The carbon nanotube aerogel was continuously wound by a rotating mandrel and densified by *in situ* liquid spraying of an ether aqueous solution. After liquid evaporation, a multi-layer seamless carbon nanotube film with a maximum width of 1 m was prepared.

Fabrication of DC-TING

The DC-TING had an area of 1 cm^2 and a volume of 0.03 cm^3. The thickness of both the carbon nanotube film and the PTFE film constituting the DC-TING are 100 μm. The surface of the PTFE film was microscopically engraved by a laser engraving machine (Speedy 300, Trotec, Marchtrenk, Austria), and the laser had a power of 3 W and an engraving speed of 1 cm/s. Plasma sputtering on PTFE surfaces was carried on by a plasma cleaner (CPC-A, CIF, Beijing, China) with a sputtering power of 50 W and a treatment time of 30 s.

Electrical measurement

The HPG operates normally with contact forces supplied by a linear motor (PL0119x600/520, LinMot, Spreitenbach, Switzerland). Its output electric signal is

collected by a test system consisting of an electrometer (6514, Keithley, Cleveland, OH, USA) and a data acquisition card (BNC-2120, National Instruments, Austin, TX, USA). The Faraday cylinder was used to test the charge of droplets and water mist.

SUPPLEMENTAL INFORMATION

Supplemental information can be found online at https://doi.org/10.1016/j.matt.2023.08.022.

ACKNOWLEDGMENTS

The authors are grateful for the support received from the National Key R&D Project from Minister of Science and Technology (2021YFA1201601) and appreciate the technical assistance from the instrument and equipment platform of the Beijing Institute of Nanoenergy and Nanosystems. In addition, we thank Feiyao Yang, Puguang Peng, and Yaowen Ouyang from the Beijing Institute of Nanoenergy and Nanosystems for their help in checking the manuscript, building experimental platforms, and shooting demonstration videos.

AUTHOR CONTRIBUTIONS

D.W. and Z.L.W. proposed the idea and the project. D.W. designed all the experiments and supervised the whole project. X.L. carried out the experiments in this paper and analyzed the corresponding data. S.L. analyzed the adjustment principle of SL in the EDL. X.G. and J.S. simulated cation and anion concentrations and total charge density of the diffuse layer with distance from the PET film surface. All the authors discussed the results and commented on the manuscript. D.W. and X.L. wrote this paper.

DECLARATION OF INTERESTS

The authors declare no competing interests.

Received: May 29, 2023
Revised: August 9, 2023
Accepted: August 28, 2023
Published: September 20, 2023

REFERENCES

1. Li, C., Hu, M., Li, Y., Jiang, H., Ge, N., Montgomery, E., Zhang, J., Song, W., Dávila, N., Graves, C.E., et al. (2017). Analogue signal and image processing with large memristor crossbars. Nat. Electron. *1*, 52–59. https://doi.org/10.1038/s41928-017-0002-z.

2. Kaspar, C., Ravoo, B.J., van der Wiel, W.G., Wegner, S.V., and Pernice, W.H.P. (2021). The rise of intelligent matter. Nature *594*, 345–355. https://doi.org/10.1038/s41586-021-03453-y.

3. Mehonic, A., and Kenyon, A.J. (2022). Brain-inspired computing needs a master plan. Nature *604*, 255–260. https://doi.org/10.1038/s41586-021-04362-w.

4. Baillet, S. (2017). Magnetoencephalography for brain electrophysiology and imaging. Nat. Neurosci. *20*, 327–339. https://doi.org/10.1038/nn.4504.

5. Rao, S.M., Mayer, A.R., and Harrington, D.L. (2001). The evolution of brain activation during temporal processing. Nat. Neurosci. *4*, 317–323. https://doi.org/10.1038/85191.

6. Wang, H., Fan, Y., Hou, Y., Chen, B., Lei, J., Yu, S., Chen, X., and Hou, X. (2022). Host-guest liquid gating mechanism with specific recognition interface behavior for universal quantitative chemical detection. Nat. Commun. *13*, 1906. https://doi.org/10.1038/s41467-022-29549-1.

7. Hou, Y., and Hou, X. (2021). Bioinspired nanofluidic iontronics. Science *373*, 628–629. https://doi.org/10.1126/science.abj0437.

8. Xiong, T., Li, C., He, X., Xie, B., Zong, J., Jiang, Y., Ma, W., Wu, F., Fei, J., Yu, P., and Mao, L. (2023). Neuromorphic functions with a polyelectrolyte-confined fluidic memristor. Science *379*, 156–161. https://doi.org/10.1126/science.adc9150.

9. Maier, J. (2005). Nanoionics: ion transport and electrochemical storage in confined systems. Nat. Mater. *4*, 805–815. https://doi.org/10.1038/nmat1513.

10. Sarpeshkar, R. (1998). Analog versus digital: extrapolating from electronics to neurobiology. Neural Comput. *10*, 1601–1638. https://doi.org/10.1162/089976698300017052.

11. Bisri, S.Z., Shimizu, S., Nakano, M., and Iwasa, Y. (2017). Endeavor of Iontronics: From Fundamentals to Applications of Ion-Controlled Electronics. Adv. Mater. *29*, 1607054. https://doi.org/10.1002/adma.201607054.

12. Béguin, F., Presser, V., Balducci, A., and Frackowiak, E. (2014). Carbons and electrolytes for advanced supercapacitors. Adv. Mater. *26*, 2219–2251. https://doi.org/10.1002/adma.201304137.

13. Yang, J., Shin, J., Park, M., Lee, G.-H., Amedzo-Adore, M., and Kang, Y.-M. (2017). The synergistic effect of nitrogen doping and para-phenylenediamine functionalization on the

physicochemical properties of reduced graphene oxide for electric double layer supercapacitors in organic electrolytes. J. Mater. Chem. A *5*, 12426–12434. https://doi.org/10.1039/c7ta03194g.

14. Wang, Y., Liang, B., Zhu, J., Li, G., Li, Q., Ye, R., Fan, J., and Zhi, C. (2023). Manipulating electric double layer adsorption for stable solid-electrolyte interphase in 2.3 Ah Zn-pouch cells. Angew. Chem. Int. Ed. *62*, e202302583. https://doi.org/10.1002/anie.202302583.

15. Zhou, Y., Su, M., Yu, X., Zhang, Y., Wang, J.-G., Ren, X., Cao, R., Xu, W., Baer, D.R., Du, Y., et al. (2020). Real-time mass spectrometric characterization of the solid-electrolyte interphase of a lithium-ion battery. Nat. Nanotechnol. *15*, 224–230. https://doi.org/10.1038/s41565-019-0618-4.

16. Butler, J.A.V. (1948). Theory of the stability of lyophobic colloids. Nature *162*, 315–316. https://doi.org/10.1038/162315b0.

17. Zhang, W., Lu, Y., Wan, L., Zhou, P., Xia, Y., Yan, S., Chen, X., Zhou, H., Dong, H., and Liu, K. (2022). Engineering a passivating electric double layer for high performance lithium metal batteries. Nat. Commun. *13*, 2029. https://doi.org/10.1038/s41467-022-29761-z.

18. Lin, S., Chen, X., and Wang, Z.L. (2022). Contact electrification at the liquid-solid interface. Chem. Rev. *122*, 5209–5232. https://doi.org/10.1021/acs.chemrev.1c00176.

19. Helmholtz, H. (1853). Ueber einige Gesetze der Vertheilung elektrischer Ströme in körperlichen Leitern mit Anwendung auf die thierisch-elektrischen Versuche. Ann. Phys. *165*, 211–233. https://doi.org/10.1002/andp.18531650603.

20. Gouy, M. (1910). Sur la constitution de la charge électrique à la surface d'un électrolyte. J. Phys. Theor. Appl. *9*, 457–468. https://doi.org/10.1051/jphystap:019100090045700.

21. Chapman, D.L. (1913). A contribution to the theory of electrocapillarity. Philos. Mag. A *25*, 475–481. https://doi.org/10.1080/14786440408634187.

22. Stern, O. (1924). The theory of the electric double layer. Z. Elektrochem. Angew. Phys. Chem. *30*, 508–516. https://doi.org/10.1002/bbpc.192400182.

23. Grahame, D.C. (1947). The electrical double layer and the theory of electrocapillarity. Chem. Rev. *41*, 441–501. https://doi.org/10.1021/cr60130a002.

24. Heo, J., Ahn, H., Won, J., Son, J.G., Shon, H.K., Lee, T.G., Han, S.W., and Baik, M.-H. (2020). Electro-inductive effect: Electrodes as functional groups with tunable electronic properties. Science *370*, 214–219. https://doi.org/10.1126/science.abb6375.

25. Aragonès, A.C., Haworth, N.L., Darwish, N., Ciampi, S., Bloomfield, N.J., Wallace, G.G., Diez-Perez, I., and Coote, M.L. (2016). Electrostatic catalysis of a Diels-Alder reaction. Nature *531*, 88–91. https://doi.org/10.1038/nature16989.

26. Wang, Z.L., and Wang, A.C. (2019). On the origin of contact-electrification. Mater. Today *30*, 34–51. https://doi.org/10.1016/j.mattod.2019.05.016.

27. Lin, S., Xu, L., Chi Wang, A., and Wang, Z.L. (2020). Quantifying electron-transfer in liquid-solid contact electrification and the formation of electric double-layer. Nat. Commun. *11*, 399. https://doi.org/10.1038/s41467-019-14278-9.

28. Nie, J., Ren, Z., Xu, L., Lin, S., Zhan, F., Chen, X., and Wang, Z.L. (2020). Probing contact-electrification-induced electron and ion transfers at a liquid-solid interface. Adv. Mater. *32*, e1905696. https://doi.org/10.1002/adma.201905696.

29. Qiao, G., Wang, J., Yu, X., Jia, R., Cheng, T., and Wang, Z.L. (2021). A bidirectional direct current triboelectric nanogenerator with the mechanical rectifier. Nano Energy *79*, 105408. https://doi.org/10.1016/j.nanoen.2020.105408.

30. Zhang, C., Zhou, T., Tang, W., Han, C., Zhang, L., and Wang, Z.L. (2014). Rotating-disk-based direct-current triboelectric nanogenerator. Adv. Energy Mater. *4*, 1301798. https://doi.org/10.1002/aenm.201301798.

31. Li, X.D., Cao, H.J., Xie, S.Y., Li, K.C., Liu, K.Y., Tao, F.B., Yang, L.S., Zhou, L., Wang, J., and Wang, Z.L. (2022). A highly efficient constant-voltage triboelectric nanogenerator. Psychol. Health Med. *27*, 1334–1346. https://doi.org/10.1039/d1ee03961j.

32. Ryu, H., Lee, J.H., Khan, U., Kwak, S.S., Hinchet, R., and Kim, S.-W. (2018). Sustainable direct current powering a triboelectric nanogenerator via a novel asymmetrical design. Energy Environ. Sci. *11*, 2057–2063. https://doi.org/10.1039/c8ee00188j.

33. Liu, D., Yin, X., Guo, H., Zhou, L., Li, X., Zhang, C., Wang, J., and Wang, Z.L. (2019). A constant current triboelectric nanogenerator arising from electrostatic breakdown. Sci. Adv. *5*, eaav6437. https://doi.org/10.1126/sciadv.aav6437.

34. Yoon, H.J., Kang, M., Seung, W., Kwak, S.S., Kim, J., Kim, H.T., and Kim, S.W. (2020). Microdischarge-based direct current triboelectric nanogenerator via accumulation of triboelectric charge in atmospheric condition. Adv. Energy Mater. *10*, 2000730. https://doi.org/10.1002/aenm.202000730.

35. Liu, J., Zhang, Y., Chen, J., Bao, R., Jiang, K., Khan, F., Goswami, A., Li, Z., Liu, F., Feng, K., et al. (2019). Separation and quantum tunneling of photo-generated carriers using a tribo-Induced field. Matter *1*, 650–660. https://doi.org/10.1016/j.matt.2019.05.017.

36. Zhang, Z., Wang, Z., Chen, Y., Feng, Y., Dong, S., Zhou, H., Wang, Z.L., and Zhang, C. (2022). Semiconductor contact-electrification-dominated tribovoltaic effect for ultrahigh power generation. Adv. Mater. *34*, e2200146. https://doi.org/10.1002/adma.202200146.

37. Wang, H., Xu, L., Bai, Y., and Wang, Z.L. (2020). Pumping up the charge density of a triboelectric nanogenerator by charge-shuttling. Nat. Commun. *11*, 4203. https://doi.org/10.1038/s41467-020-17891-1.

38. Liu, Z., Huang, Y., Shi, Y., Tao, X., He, H., Chen, F., Huang, Z.-X., Wang, Z.L., Chen, X., and Qu, J.-P. (2022). Fabrication of triboelectric polymer films via repeated rheological forging for ultrahigh surface charge density. Nat. Commun. *13*, 4083. https://doi.org/10.1038/s41467-022-31822-2.

39. Wang, J., Wu, C., Dai, Y., Zhao, Z., Wang, A., Zhang, T., and Wang, Z.L. (2017). Achieving ultrahigh triboelectric charge density for efficient energy harvesting. Nat. Commun. *8*, 88. https://doi.org/10.1038/s41467-017-00131-4.

40. Fu, J., Xu, G., Li, C., Xia, X., Guan, D., Li, J., Huang, Z., and Zi, Y. (2020). Achieving ultrahigh output energy density of triboelectric nanogenerators in high-pressure gas environment. Adv. Sci. *7*, 2001757. https://doi.org/10.1002/advs.202001757.

41. Wen, R., Guo, J., Yu, A., Zhai, J., and Wang, Z.L. (2019). Humidity-resistive triboelectric nanogenerator fabricated using metal organic framework composite. Adv. Funct. Mater. *29*, 1807655. https://doi.org/10.1002/adfm.201807655.

42. Xu, S., Ding, W., Guo, H., Wang, X., and Wang, Z.L. (2019). Boost the performance of triboelectric nanogenerators through circuit oscillation. Adv. Energy Mater. *9*, 1900772. https://doi.org/10.1002/aenm.201900772.

43. Zargari, S., Rezania, A., Koozehkanani, Z.D., Veladi, H., Sobhi, J., and Rosendahl, L. (2022). Effect of the inherent capacitance optimization on the output performance of triboelectric nanogenerators. Nano Energy *92*, 106740. https://doi.org/10.1016/j.nanoen.2021.106740.

44. Bockris, J.O.M., Devanathan, M.A.V., and Müller, K. (1965). On the structure of charged interfaces. Electrochemistry *832*, 832–863. https://doi.org/10.1016/B978-1-4831-9831-6.50068-0.

45. Lyons, L.E., and Mackie, J.C. (1963). Electron-donating properties of central sympathetic suppressants. Nature *197*, 589. https://doi.org/10.1038/197589a0.

46. Zhou, Y., Hao, Y., Sun, P., Chen, M., Zhang, T., and Wu, H. (2022). Relationship among surface electric double layer of cardiomyocyte membrane and toxicology of digoxin and opening of ion channels. Sci. Rep. *12*, 20749. https://doi.org/10.1038/s41598-022-25205-2.